

Foundations of MIMO Radar Detection Aided by Reconfigurable Intelligent Surfaces

Stefano Buzzi, *Senior Member, IEEE*, Emanuele Grossi, *Senior Member, IEEE*, Marco Lops, *Fellow, IEEE*, Luca Venturino, *Senior Member, IEEE*

Abstract—A reconfigurable intelligent surface (RIS) is a nearly-passive flat layer made of inexpensive elements that can add a tunable phase shift to the impinging electromagnetic wave and are controlled by a low-power electronic circuit. This paper considers the fundamental problem of target detection in a RIS-aided multiple-input multiple-output (MIMO) radar. At first, a general signal model is introduced, which includes the possibility of using up to two RISs (one close to the radar transmitter and one close to the radar receiver) and subsumes both a monostatic and a bistatic radar configuration with or without a line-of-sight view of the prospective target. Upon resorting to a generalized likelihood ratio test (GLRT), the design of the phase shifts introduced by the RIS elements is formulated as the maximization of the probability of detection in the location under inspection for a fixed probability of false alarm, and suitable optimization algorithms are proposed. The performance analysis shows the benefits granted by the presence of the RISs and shed light on the interplay among the key system parameters, such as the radar-RIS distance, the RIS size, and location of the prospective target. A major finding is that the RISs should be better deployed in the near-field of the radar arrays at both the transmit and the receive side. The paper is concluded by discussing some open problems and foreseen applications.

Index Terms—MIMO Radar, LOS/NLOS, Bi/Mono-Static, Target Detection, Reconfigurable Intelligent Surfaces.

I. INTRODUCTION

Reconfigurable intelligent surfaces (RISs) are attracting a huge interest from researchers, as they allow to realize smart radio environments [1]–[3]. An RIS is a nearly-passive low-cost planar structure made of engineered materials with tunable electromagnetic characteristics; current implementations include reflectarrays, transmitarrays, liquid crystal surfaces, and software-defined meta-surfaces [4]–[6]. Such device does not emit any power of its own and only aims to manipulate existing waves to alter the wireless propagation channel. An RIS differs from a specular reflector or a scattering object, as its elements can be individually controlled by a low-power external logic to

redirect the incident electromagnetic wave towards an arbitrary (anomalous) direction or a specific location. This focusing mechanism resembles that of a phased array and can enhance the signal reception at a desired destination. Differently from amplify-and-forward relaying, the signal boost is obtained without using a radio-frequency chain or consuming power for amplification¹ or adding a processing delay/noise or requiring a half-duplex operation [9]. In light of their low hardware footprint, the RISs can be easily deployed in the environment; for example, they can be integrated into the facades and the roof of a building, the walls and the ceiling of a room, and the case of a laptop. RIS-empowered radio environments can be exploited in all kind of wireless services, including communication, localization, and radar operations, opening up new opportunities. As it is meaningful to create an RIS-aided indirect link only if the cascade of the source-RIS and RIS-destination channels is sufficiently good, the system engineer must preliminarily verify a good location for the RIS placement.

In the past years, the RISs have been mainly investigated in wireless communications to enhance the network performance. In [10], a RIS assists the communications between a multi-antenna base station (BS) and multiple single-antenna users, and the total transmit power is minimized via joint active and passive beamforming, subject to a signal-to-interference-plus-noise ratio (SINR) constraint for each user. In [11], the phase shifts of the RIS can only take value in a finite set, and the relation between the set cardinality and the rate degradation is investigated. In [12], the phase shifts of the RIS are employed in conjunction with the communication transmitter to encode a message, showing that this scheme achieves a larger capacity than that obtained when the RIS is designed only to maximize the received signal-to-noise ratio (SNR). The work in [13], instead, considers a point-to-point multiple-input multiple-output (MIMO) link and performs an alternating optimization of the transmit precoder and the phase shifts of the RIS to minimize the symbol error rate. The channel estimation in a RIS-aided link has been tackled in [14], while other studies have assessed the RIS benefits in the context of wireless power transfer [15], antenna design [16], and coverage extension [17]. The reader may refer to [1]–[3] for a more comprehensive overview.

The RISs can also be exploited for user localization in mobile networks [18]. In [19], a scenario with one BS, one mobile device, and one RIS is considered, and the achievable localization and orientation performance with synchronous and

The work of S. Buzzi, E. Grossi and L. Venturino was supported by the research program “Dipartimenti di Eccellenza 2018–2022” sponsored by the Italian Ministry of Education, University, and Research (MIUR).

S. Buzzi, E. Grossi and L. Venturino are with the Department of Electrical and Information Engineering (DIEI), University of Cassino and Southern Lazio, 03043 Cassino, Italy, and with Consorzio Nazionale Interuniversitario per le Telecomunicazioni, 43124 Parma, Italy (e-mail: buzzi@unicas.it; e.grossi@unicas.it; l.venturino@unicas.it).

M. Lops is with the Department of Electrical and Information Technology (DIETI), University of Naples Federico II, 80138 Naples, Italy, and with Consorzio Nazionale Interuniversitario per le Telecomunicazioni, 43124 Parma, Italy (e-mail: lops@unina.it).

Part of this work has been submitted for possible presentation at the 2022 IEEE Radar Conference and the 2022 International Conference on Acoustics, Speech, & Signal Processing.

¹Active RISs able to amplify and redirect the incident electromagnetic signal have been studied in [7], [8] to compensate for the two-hop attenuation in the RIS-aided link; however, these surfaces are not considered here.

asynchronous signalling schemes are studied. The use of an RIS may also allow to perform joint synchronization and localization without using two-way transmission, even if the mobile user is equipped with one antenna [20]. The problem of joint localization and communication is instead considered in [21], which presents an RIS design based on the use of hierarchical codebooks and feedback from the mobile station.

More recently, researchers have started investigating the RIS benefits in dual-function radar-communication (DFRC) systems. In [22], the radar detection probability is maximized by optimizing the transmit beamformer of the BS and the phase shifts of the RIS, subject to SINR and power constraints. Instead, the transmit waveforms of the BS and the phase shifts of the RIS are chosen in [23] to mitigate the multiuser interference under a beam pattern constraint.

With regard to the fundamental problem of radar target detection, in our earlier contribution [24] we assumed that the radar is capable of forming (a) two transmit beams pointing towards the prospective target and the RIS and one receive beam pointing towards the prospective target only or, viceversa, (b) one transmit beam pointing towards the prospective target only and two receive beams pointing towards the prospective target and the RIS. Under such a scenario, a theoretical analysis is carried out for closely- and widely-spaced (with respect to the location of the prospective target) radar and RIS deployments, showing that large gains can be provided by the nearby RIS, and initial hints on the optimal RIS placement are provided. In [25], the case where no direct path between the radar and the prospective target exists is considered, mimicking the companion situation where the RIS provides an indirect link between a communication source and a destination that would be otherwise not reachable. Finally, [26] represents a first contribution to the scenario considered here and, although passing over a number of relevant effects and situations, as detailed in the sequel of this contribution, makes the basic point that an RIS can indeed aid the MIMO radar detection.

A. Contribution and paper structure

The bottom line of the current studies is that suitably deployed RISs can modify the wireless channel response, thus providing novel degrees of freedom to the system design. In this work, we focus on the classical target detection problem [27]–[29] and investigate under which conditions the RISs may boost the performance of an MIMO radar with closely-spaced antennas, while preserving its key functions, i.e., illuminating a large angular sector and focusing on a desired point by only relying on receive signal processing. For a given RIS size, the distance covered by its re-directed wave is tied to the power of the incident wave, which in turn depends on the power emitted by the active source and the length of the source-RIS hop. Accordingly, several usage contexts are possible: for example, radars for air-traffic, coastal, and marine surveillance could be aided by nearby RISs deployed on the same structure hosting the radar, a nearby building/wall, or the ground itself, while wireless access points with integrated radar and communication capabilities can use the same RISs to support both functions.

With reference to the scenarios outlined in Fig. 1, we first derive a novel signal model, wherein the MIMO radar transmits a set of orthogonal waveforms and, assisted by a *forward* and/or a *backward* RIS operating as a reflecting mirror, verifies the presence/absence of a prospective target in a given location under inspection. The model includes monostatic, bistatic, line-of-sight (LOS), and non-line-of-sight (NLOS) radar configurations and accounts for the presence of up to four paths from the transmitter to the prospective target to the receiver. Also, we distinguish among the two relevant situations that the forward and backward RISs are in the near- or far-field of the radar transmitter and receiver, respectively.

Next, we derive the generalized likelihood ratio test (GLRT) receiver with respect to the unknown target response and tackle the design of the phase shifts introduced by the reflecting elements by maximizing the target detection probability for a fixed probability of false alarm: interestingly, the optimization problem turns out to be *separable*, i.e., the forward and backward RISs can be designed independently. Also, if the forward (backward) RIS and radar transmitter (receiver) are in each other's far-field the optimum phase shifts are found in closed form; instead, in a near-field situation, the optimization problem is strongly NP-hard in general and can be approximately solved through an alternate maximization or by resorting to a convex relaxation. Interestingly, this latter approach provides a randomized solution whose expected value is at least $\pi/4 \approx 0.785$ times the optimum. The special case in which the radar is monostatic and the same RIS provides both a forward and a backward indirect path is also examined, and an ad-hoc algorithm to select the phase shift of each reflecting element is proposed.

A performance analysis has been carried out to assess the impact of the radar-RIS distance, the RIS size, and the location under inspection. The results show that only a marginal gain (as compared to the case where the radar operates alone) can be obtained if radar and RIS are in each other's far-field; this confirms the intuition in [24] that an RIS should be better placed in proximity of the radar transmitter or receiver. Conversely, a large performance gain can be obtained under a near-field radar-RIS deployment; interestingly, such gain almost doubles when the prospective target is in the view of both the forward and backward RISs, as compared to the case where only a single surface illuminates/observes it. The performance of a monostatic radar with a single RIS (the simplest and perhaps most realistic and cost-effective configuration) is also contrasted to that of an *ideal* system where the phase shifts of the reflecting elements are changed in between the transmission and reception phases, showing that these configurations are substantially equivalent.

The paper is organized as follows. In Sec. II, the system description is presented. In Sec. III, the design of the phase shifts introduced by the RIS elements is studied. In Sec. IV, some examples are given to assess the performance of an RIS-aided radar. Finally, concluding remarks and hints for future developments are provided in Sec. V.

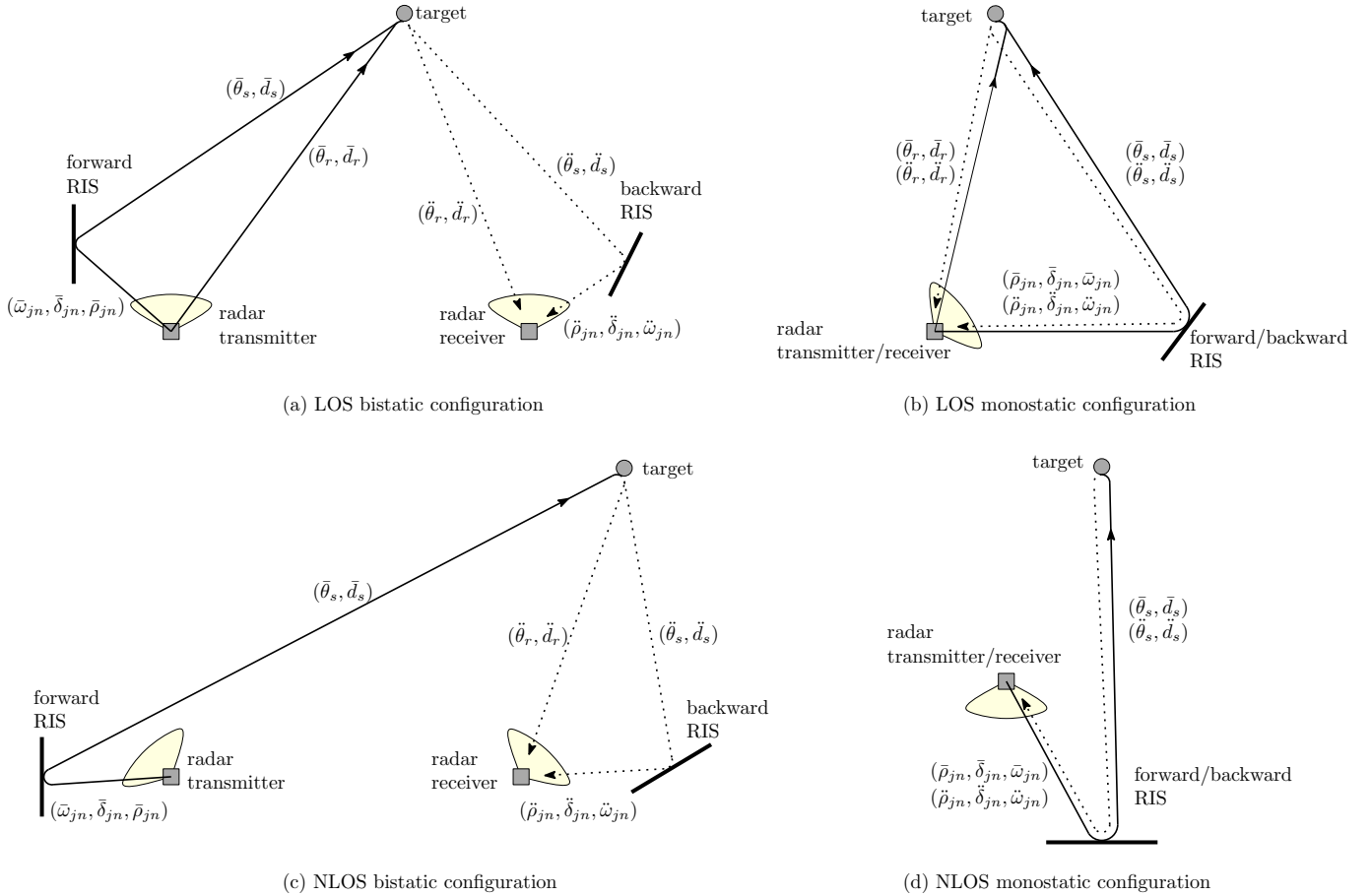


Figure 1. Examples of bistatic and monostatic system geometries. In configurations (a) and (b), the radar transmitter and receiver have a LOS view of the prospective target; the indirect paths granted by forward/backward RISs can be exploited here to improve the performance that the radar would have alone. In configuration (c), the radar transmitter does not have a LOS view of the prospective target; the forward RIS grants here a NLOS path for its illumination. In configuration (d), the radar only relies on the forward/backward RISs to illuminate the prospective target and capture its echo.

B. Notation

Column vectors and matrices are denoted by lowercase and uppercase boldface letters, respectively. The symbols $(\cdot)^*$, $(\cdot)^T$ and $(\cdot)^H$ denote conjugate, transpose, and conjugate-transpose, respectively. \mathbf{I}_M is a $M \times M$ identity matrix, while A_{ij} and a_i denote the (i, j) -th entry of the matrix \mathbf{A} and the i -th entry of the vector \mathbf{a} , respectively. $\mathbf{A} \succeq 0$ means that \mathbf{A} is Hermitian positive semidefinite. $\text{Tr}\{\mathbf{A}\}$ and $\|\mathbf{a}\|$ denote the trace of the square matrix \mathbf{A} and the Frobenius norm of the vector \mathbf{a} , respectively. $\text{rank}\{\mathbf{A}\}$ is the rank of the matrix \mathbf{A} . $\text{diag}\{\mathbf{a}\}$ is the $M \times M$ matrix containing the entries of M -dimensional vector \mathbf{a} on the main diagonal and zero elsewhere. The symbol \otimes denotes the Kronecker product, $\mathbb{E}[\cdot]$ the statistical expectation, and j the imaginary unit.

II. SYSTEM DESCRIPTION

We consider an RIS-aided MIMO radar aimed to detect a prospective target in a given location under inspection. The radar transmitter and receiver are equipped with $\bar{N}_r \geq 1$ and $\check{N}_r \geq 1$ closely-spaced elements, respectively, arranged into a planar array;² the building element of each array can

be a single antenna or a subarray module composed itself of multiple antennas. The radar emits \bar{N}_r orthogonal and equal-power waveforms, one from each radiating element. A planar RIS (referred to as the forward RIS) can help the radar transmitter illuminate the prospective target; this surface is composed of $\bar{N}_s \geq 1$ elements, also called unit cells or meta atoms, that can change the phase of the incident electromagnetic field while reflecting it. Similarly, a planar RIS (referred to as the backward RIS) with $\check{N}_s \geq 1$ tunable reflecting elements can help the radar receiver capture the power scattered by a target.³ A data link is assumed to exist between the radar control unit, where the system design is carried out, and each RIS.

The RISs can modify the response of the environment to the waveforms emitted by the radar; in particular, a prospective target can be illuminated by the radar transmitter (direct path) and/or by the forward RIS (indirect path); likewise, the reflections originated by the target may reach the radar receiver through a direct path and/or an indirect path bouncing on the backward RIS. As shown in Fig. 1, up to four echoes may be observed, corresponding to a direct illumination and a

²Henceforth, the diacritical marks $(\bar{\cdot})$ and $(\check{\cdot})$ are used to distinguish between the transmit and receive sides, respectively: this notation mimics the solid and dotted line-styles adopted in Fig. 1.

³The following signal model and design methodology still remain valid if each RIS element retransmits (rather than reflects) a phase-shifted version of the incident electromagnetic field [16].

direct reflection, an indirect illumination and a direct reflection, a direct illumination and an indirect reflection, and an indirect illumination and an indirect reflection. The model considered in this work (see Section II-C) encompasses both a bistatic and a monostatic radar; in this latter case, the forward and backward RISs may collapse into a single surface redirecting the incident waves from the radar transmitter and the target, as shown in Figs. 1(b)-(d). Also, the model encompasses both a LOS and a NLOS radar; in the former case, both the transmitter and the receiver already have a direct view of the prospective target and the additional RIS-assisted paths can be exploited to improve the performance that the radar would have alone; in the latter case, the indirect paths granted by the RISs may extend the field of view of the radar, as shown in Figs. 1(c)-(d). We underline that the configuration in Fig. 1(d) may be of interest also to replace an expensive radar transceiver that would be required to cover the region of interest with a low-cost feeder that sends/receives signals via a re-configurable surface capable of electronically-tunable beamforming [24].

A. Geometric parameters

The transmit/receive/reflecting arrays are located on the (y, z) -plane of a Cartesian local reference system, with elements oriented towards the positive x -axis. At the transmit side, we define the following quantities:⁴

- \bar{d}_r , $\bar{\theta}_r^{\text{az}}$, and $\bar{\theta}_r^{\text{el}}$ are the range and the azimuth and elevation angles of the target from the reference element of the transmit array of the radar, respectively;
- \bar{d}_s , $\bar{\theta}_s^{\text{az}}$, and $\bar{\theta}_s^{\text{el}}$ are the range and the azimuth and elevation angles of the target from the reference element of the forward RIS, respectively;
- $\bar{\delta}$, $\bar{\rho}^{\text{az}}$, $\bar{\rho}^{\text{el}}$, $\bar{\omega}^{\text{az}}$, $\bar{\omega}^{\text{el}}$ are the length, the azimuth and elevation angles of departure, and the azimuth and elevation angles of arrival, respectively, of the path from the reference element of the radar transmitter to the reference element of the forward RIS;
- $\bar{\delta}_{jn}$, $\bar{\rho}_{jn}^{\text{az}}$, $\bar{\rho}_{jn}^{\text{el}}$, $\bar{\omega}_{jn}^{\text{az}}$, and $\bar{\omega}_{jn}^{\text{el}}$ are the length, the azimuth and elevation angles of departure, and the azimuth and elevation angles of arrival, respectively, of the path from the j -th element of the radar transmitter to the n -th element of the forward RIS, respectively; clearly, $\bar{\delta}_{jn} = \bar{\delta}$, $\bar{\rho}_{jn}^{\text{az}} = \bar{\rho}^{\text{az}}$, $\bar{\rho}_{jn}^{\text{el}} = \bar{\rho}^{\text{el}}$, $\bar{\omega}_{jn}^{\text{az}} = \bar{\omega}^{\text{az}}$, and $\bar{\omega}_{jn}^{\text{el}} = \bar{\omega}^{\text{el}}$ if the j -th transmit and the n -th forward reflecting element are the reference one of the corresponding array.

Similar parameters are defined at the receive side, with an obvious modification of the notation, i.e., the diacritical mark $(\bar{\cdot})$ is replaced by $(\check{\cdot})$. For brevity, we denote by $\phi = \{\phi^{\text{az}}, \phi^{\text{el}}\}$ the azimuth and elevation angles ϕ^{az} and ϕ^{el} . These parameters are summarized in Fig. 1.

⁴We follow the standard notation that the azimuth angle of a point $\mathbf{p} \in \mathbb{R}^3$ is the angle between the x -axis and the orthogonal projection of the vector pointing towards \mathbf{p} onto the (x, y) -plane, which takes values in $[-\pi, \pi)$ and is positive when going from the x -axis towards the y -axis; also, the elevation angle is the angle between the vector pointing towards \mathbf{p} and its orthogonal projection onto the (x, y) -plane, which takes values in $[-\pi/2, \pi/2)$ and is positive when going towards the positive z -axis from the (x, y) -plane.

B. Design assumptions

At the design stage, we make the following assumptions.

- There is no coupling among the elements of the considered transmit/receive/reflecting arrays.
- There is only LOS propagation in the radar-RIS, radar-target, and RIS-target hops (whenever present).
- Any pair of transmit and forward reflecting elements are in each other's far-field; similarly, any pair of receive and backward reflecting elements are in each other's far-field. This requires that [30]

$$\min_{j,n} \bar{\delta}_{jn} \geq \max\{2\bar{\Delta}_r^2/\lambda, 2\bar{\Delta}_s^2/\lambda, 5\bar{\Delta}_r, 5\bar{\Delta}_s, 1.6\lambda\} \quad (1a)$$

$$\min_{j,n} \check{\delta}_{jn} \geq \max\{2\check{\Delta}_r^2/\lambda, 2\check{\Delta}_s^2/\lambda, 5\check{\Delta}_r, 5\check{\Delta}_s, 1.6\lambda\} \quad (1b)$$

where λ is the carrier wavelength and $\bar{\Delta}_r$, $\bar{\Delta}_s$, $\check{\Delta}_r$, and $\check{\Delta}_s$ are the maximum size of each element of the transmit, forward reflecting, receive, and backward reflecting arrays, respectively. We underline that the radar transmitter and the forward RIS and, similarly, the radar receiver and the backward RIS are not required to be in each other's far-field. Accordingly, the phase curvature of the wavefront across the array elements is not neglected in the radar-RIS hops [16], [31].

- The target and any radar array are in each other's far-field, i.e., we have [30]

$$\bar{d}_r \geq \max\{2\bar{D}_t^2/\lambda, 2\bar{D}_r^2/\lambda, 5\bar{D}_t, 5\bar{D}_r, 1.6\lambda\} \quad (2a)$$

$$\check{d}_r \geq \max\{2\check{D}_t^2/\lambda, 2\check{D}_r^2/\lambda, 5\check{D}_t, 5\check{D}_r, 1.6\lambda\} \quad (2b)$$

where \bar{D}_r and \check{D}_r are the maximum size of the transmit and the receive array, respectively, and \bar{D}_t and \check{D}_t are the effective size of the target as seen from the radar transmitter and receiver, respectively; also, the target and any RIS are in each other's far-field, i.e., we have [30]

$$\bar{d}_s \geq \max\{2\bar{D}_t^2/\lambda, 2\bar{D}_s^2/\lambda, 5\bar{D}_t, 5\bar{D}_s, 1.6\lambda\} \quad (3a)$$

$$\check{d}_s \geq \max\{2\check{D}_t^2/\lambda, 2\check{D}_s^2/\lambda, 5\check{D}_t, 5\check{D}_s, 1.6\lambda\} \quad (3b)$$

where \bar{D}_s and \check{D}_s are the maximum size of the forward and backward RISs, respectively. Accordingly, the phase curvature of the wavefront is neglected along the radar-target and RIS-target hops [30], [32].

- When both the radar transmitter and the forward RIS illuminate the prospective target, they see the same aspect angle [33], i.e., $\lambda/\bar{D}_t \gg \max_{j,n} \xi_{jn}$, where ξ_{jn} is the angle formed by the line segment linking the target with the j -th transmit element and the line segment linking the target with the n -th forward reflecting element; similarly, when both the radar receiver and the backward RIS observe the prospective target, they see the same aspect angle, i.e., $\lambda/\check{D}_t \gg \max_{j,n} \xi_{jn}$, where ξ_{jn} is the angle formed by the line segment linking the target with the j -th receive element and the line segment linking the target with the n -th backward reflecting element.
- The waveforms are narrowband, so that the delays of the target echoes reaching the receiver are not resolvable.

C. Received signal

A range gating operation is at first performed by projecting the signal impinging on each receive element along a delayed version of each transmit waveform (this is tantamount to sampling the output of a filter matched to the waveform), with the delay tied to the distance of the inspected resolution cell from the transmitter and the receiver [33], [34]. The available data samples are organized into a vector $\mathbf{r} \in \mathbb{C}^{\tilde{N}_r \tilde{N}_r}$ that, in the presence of a steady target, can be modeled as

$$\mathbf{r} = e\alpha + \mathbf{w} \quad (4)$$

where $e \in \mathbb{C}^{\tilde{N}_r \tilde{N}_r}$ is the known *target signature*, tied to its location, the system geometry, and the phase shifts of the RISs (more on this infra), $\alpha \in \mathbb{C}$ accounts for the unknown target response and any other scaling factor not included in the target signature (such as, for example, the transmit power); $\mathbf{w} \in \mathbb{C}^{\tilde{N}_r \tilde{N}_r}$ is a circularity-symmetric Gaussian vector with covariance matrix $\sigma_w^2 \mathbf{I}_{\tilde{N}_r \tilde{N}_r}$, accounting for the additive noise.⁵

The target signature contains the superposition of up to four paths from the radar transmitter to the target to the radar receiver (see Fig. 1), which may involve up to two bounces off the RISs. Let $\bar{\mathbf{x}} \in \mathbb{C}^{\tilde{N}_s}$ and $\check{\mathbf{x}} \in \mathbb{C}^{\tilde{N}_s}$ be the vectors with unit modulus entries specifying the phase shifts introduced by the elements of the forward and backward RISs, respectively. Then, we have

$$\begin{aligned} e(\bar{\mathbf{x}}, \check{\mathbf{x}}) &= \underbrace{(\bar{\mathbf{v}}_r \bar{\gamma}_r) \otimes (\check{\mathbf{v}}_r \check{\gamma}_r)}_{\text{Radar} \rightarrow \text{Target} \rightarrow \text{Radar}} \\ &+ \underbrace{(\bar{\mathbf{G}} \text{diag}\{\bar{\mathbf{x}}\} \bar{\mathbf{v}}_s \bar{\gamma}_s) \otimes (\check{\mathbf{v}}_r \check{\gamma}_r)}_{\text{Radar} \rightarrow \text{RIS} \rightarrow \text{Target} \rightarrow \text{Radar}} \\ &+ \underbrace{(\bar{\mathbf{v}}_r \bar{\gamma}_r) \otimes (\check{\mathbf{G}} \text{diag}\{\check{\mathbf{x}}\} \check{\mathbf{v}}_s \check{\gamma}_s)}_{\text{Radar} \rightarrow \text{Target} \rightarrow \text{RIS} \rightarrow \text{Radar}} \\ &+ \underbrace{(\bar{\mathbf{G}} \text{diag}\{\bar{\mathbf{x}}\} \bar{\mathbf{v}}_s \bar{\gamma}_s) \otimes (\check{\mathbf{G}} \text{diag}\{\check{\mathbf{x}}\} \check{\mathbf{v}}_s \check{\gamma}_s)}_{\text{Radar} \rightarrow \text{RIS} \rightarrow \text{Target} \rightarrow \text{RIS} \rightarrow \text{Radar}} \\ &= \underbrace{(\bar{\mathbf{v}}_r \bar{\gamma}_r + \bar{\mathbf{G}} \text{diag}\{\bar{\mathbf{x}}\} \bar{\mathbf{v}}_s \bar{\gamma}_s)}_{\bar{e}(\bar{\mathbf{x}})} \otimes \underbrace{(\check{\mathbf{v}}_r \check{\gamma}_r + \check{\mathbf{G}} \text{diag}\{\check{\mathbf{x}}\} \check{\mathbf{v}}_s \check{\gamma}_s)}_{\check{e}(\check{\mathbf{x}})} \end{aligned} \quad (5)$$

where we have made explicit the dependence of the vector e upon $\bar{\mathbf{x}}$ and $\check{\mathbf{x}}$ for future developments and we have defined the symbols listed below.

- $\bar{\mathbf{v}}_r \in \mathbb{C}^{\tilde{N}_r}$ and $\check{\mathbf{v}}_r \in \mathbb{C}^{\tilde{N}_r}$ are the *direct* steering vectors of the radar transmitter and receiver towards the directions $\bar{\theta}_r$ and $\check{\theta}_r$ of the target, respectively, which are tied to the array geometry and have unit modulus entries.
- $\bar{\mathbf{v}}_s \in \mathbb{C}^{\tilde{N}_s}$ and $\check{\mathbf{v}}_s \in \mathbb{C}^{\tilde{N}_s}$ are the steering vectors of the forward and backward RISs towards the directions $\bar{\theta}_s$ and $\check{\theta}_s$ of the target, respectively, which are tied to the array geometry and have unit modulus entries.
- $\bar{\gamma}_r \in \mathbb{C}$ and $\check{\gamma}_r \in \mathbb{C}$ are the direct channels between the reference transmit element and the target and between

⁵The following developments can also be extended to the case where the covariance matrix of \mathbf{w} is full-rank and has the separable structure $E[\mathbf{w}\mathbf{w}^H] = \bar{\mathbf{C}}_w \otimes \check{\mathbf{C}}_w$, with $\bar{\mathbf{C}}_w \in \mathbb{C}^{\tilde{N}_r \times \tilde{N}_r}$ and $\check{\mathbf{C}}_w \in \mathbb{C}^{\tilde{N}_r \times \tilde{N}_r}$.

Table I
POSSIBLE SYSTEM CONFIGURATIONS

Radar	$\bar{\gamma}_r$	$\check{\gamma}_r$	$\bar{\gamma}_s$	$\check{\gamma}_s$	Target	
					illuminated by	observed by
LOS	$\neq 0$	$\neq 0$	$\neq 0$	$\neq 0$	Radar & RIS	Radar & RIS
			$= 0$	$\neq 0$	Radar	Radar & RIS
			$\neq 0$	$= 0$	Radar & RIS	Radar
			$= 0$	$= 0$	Radar	Radar
NLOS	$\neq 0$	$= 0$	$\neq 0$	$\neq 0$	Radar & RIS	RIS
			$= 0$	$\neq 0$	Radar	RIS
			$= 0$	$= 0$	RIS	RIS
			$= 0$	$\neq 0$	RIS	Radar & RIS
			$\neq 0$	$= 0$	RIS	Radar

the target and the reference receive element, respectively, which account for the radar element gain, the path-loss, and the phase delay.

- $\bar{\gamma}_s \in \mathbb{C}$ and $\check{\gamma}_s \in \mathbb{C}$ are the two-hop indirect channels from the reference transmit element to the reference forward reflecting element to the target and from the target to the reference backward reflecting element to the reference receive element, respectively, which account for the radar element gain, the bistatic radar cross-section (RCS) of the reflecting element, and the two-hop path-loss and phase delay. Hereafter, we assume that $\bar{\gamma}_s = 0$ if the forward RIS is not present; similarly, $\check{\gamma}_s = 0$ if the backward RIS is not present.
- $\bar{\mathbf{G}} \in \mathbb{C}^{\tilde{N}_r \times \tilde{N}_s}$ and $\check{\mathbf{G}} \in \mathbb{C}^{\tilde{N}_r \times \tilde{N}_s}$ are the normalized channel matrices between the radar transmitter and the forward RIS and between the backward RIS and the radar receiver, respectively, whose entries account for the radar element gain, the bistatic RCS of the reflecting element, the path-loss, and the phase delay; the normalization is with respect to the scalar channel between the reference elements of the arrays that is included in $\bar{\gamma}_s$ and $\check{\gamma}_s$.

Depending on the values of $\bar{\gamma}_r$, $\check{\gamma}_r$, $\bar{\gamma}_s$, and $\check{\gamma}_s$, only some of the echoes in (5) are actually present: the possible system configurations are outlined in Table I. Our model subsumes the one considered in [26], wherein the radar has a LOS-view of the prospective target (i.e., $\bar{\gamma}_r \check{\gamma}_r \neq 0$) and only uses a backward RIS (i.e., $\bar{\gamma}_s = 0$ and $\check{\gamma}_s \neq 0$). Also, notice that $e(\bar{\mathbf{x}}, \check{\mathbf{x}})$ possesses a Kronecker structure, wherein $\bar{\mathbf{G}} \text{diag}\{\bar{\mathbf{x}}\} \bar{\mathbf{v}}_s$ and $\check{\mathbf{G}} \text{diag}\{\check{\mathbf{x}}\} \check{\mathbf{v}}_s$ are the *indirect* steering vectors of the radar transmitter and receiver towards the target via the RIS-assisted path.⁶ Accordingly, $\bar{e}(\bar{\mathbf{x}})$ is the *transmit target signature*, resulting from the superposition of the direct and indirect steering vectors of the radar transmitter towards the target with weights equal to the corresponding channels $\bar{\gamma}_r$ and $\bar{\gamma}_s$, while $\check{e}(\check{\mathbf{x}})$ is the *receive target signature*, resulting from the superposition of the direct and indirect steering vectors of the radar receiver towards the target with weights equal to the corresponding channels $\check{\gamma}_r$ and $\check{\gamma}_s$.

⁶We use here the term “steering vector” with some abuse of notation as the entries of $\bar{\mathbf{G}} \text{diag}\{\bar{\mathbf{x}}\} \bar{\mathbf{v}}_s$ and $\check{\mathbf{G}} \text{diag}\{\check{\mathbf{x}}\} \check{\mathbf{v}}_s$ may not have a unit modulus.

D. Channel model

The design methodology proposed in the following section is independent of the model adopted for the radar-target and the radar-RIS-target channels (both ways), as long as the received signal can be written as in (4) and (5). Exact modeling of an RIS-assisted channel is a non-trivial and still debated problem. In order to shed some light on the potential advantages granted by the RISs in the MIMO radar target detection, at the analysis stage we just leverage and adapt basic models so far elaborated for RIS-aided communications.

According to the standard radar equation [28], [35], the scalar channels $\bar{\gamma}_r$, $\check{\gamma}_s$, $\check{\gamma}_r$, and $\check{\gamma}_s$ are modeled as

$$\bar{\gamma}_r = \left(\frac{\bar{G}(\bar{\theta}_r)}{4\pi\bar{d}_r^2\bar{L}_r} \right)^{1/2} e^{-i2\pi\bar{d}_r/\lambda} \quad (6a)$$

$$\check{\gamma}_r = \left(\frac{\check{G}(\check{\theta}_r)\lambda^2}{(4\pi)^2\check{d}_r^2\check{L}_r} \right)^{1/2} e^{-i2\pi\check{d}_r/\lambda} \quad (6b)$$

$$\bar{\gamma}_s = \left(\frac{\bar{G}(\bar{\rho})\bar{\zeta}(\bar{\omega}, \bar{\theta}_s)}{(4\pi)^2\bar{\delta}^2\bar{d}_s^2\bar{L}_s} \right)^{1/2} e^{-i2\pi(\bar{\delta}+\bar{d}_s)/\lambda} \quad (6c)$$

$$\check{\gamma}_s = \left(\frac{\check{\zeta}(\check{\theta}_s, \check{\omega})\check{G}(\check{\rho})\lambda^2}{(4\pi)^3\check{d}_s^2\check{\delta}^2\check{L}_s} \right)^{1/2} e^{-i2\pi(\check{d}_s+\check{\delta})/\lambda} \quad (6d)$$

where $\bar{G}(\varphi)$ and $\check{G}(\varphi)$ are the gain of the transmit and receive elements in the direction $\varphi = \{\varphi^{\text{az}}, \varphi^{\text{el}}\}$, respectively, $\bar{\zeta}(\varphi_{\text{in}}, \varphi_{\text{out}})$ and $\check{\zeta}(\varphi_{\text{in}}, \varphi_{\text{out}})$ are the bistatic RCS of the forward and backward reflecting elements towards the direction $\varphi_{\text{out}} = \{\varphi_{\text{out}}^{\text{az}}, \varphi_{\text{out}}^{\text{el}}\}$ when illuminated from the direction $\varphi_{\text{in}} = \{\varphi_{\text{in}}^{\text{az}}, \varphi_{\text{in}}^{\text{el}}\}$, respectively, and \bar{L}_r , \check{L}_r , \bar{L}_s , and \check{L}_s are loss factors accounting for any additional attenuation along the corresponding paths, respectively.

Following [16], [31], the entries of channel matrix \bar{G} are modeled as $\bar{G}_{jn} = 0$, if $\bar{\gamma}_s = 0$, and

$$\bar{G}_{jn} = \left(\frac{\bar{G}(\bar{\rho}_{jn})\bar{\zeta}(\bar{\omega}_{jn}, \bar{\theta}_s)\bar{\delta}^2}{\bar{G}(\bar{\rho})\bar{\zeta}(\bar{\omega}, \bar{\theta}_s)\bar{\delta}_{jn}^2} \right)^{1/2} e^{-i2\pi(\bar{\delta}_{jn}-\bar{\delta})/\lambda} \quad (7)$$

otherwise. In this latter case, $\bar{G}_{jn} = 1$, if the j -th transmit and the n -th forward reflecting element are the reference ones of the corresponding arrays, in keeping with (6). Similarly, the entries of \check{G} are modeled as $\check{G}_{jn} = 0$, if $\check{\gamma}_s = 0$, and

$$\check{G}_{jn} = \left(\frac{\check{\zeta}(\check{\theta}_s, \check{\omega}_{jn})\check{G}(\check{\rho}_{jn})\check{\delta}^2}{\check{\zeta}(\check{\theta}_s, \check{\omega})\check{G}(\check{\rho})\check{\delta}_{jn}^2} \right)^{1/2} e^{-i2\pi(\check{\delta}_{jn}-\check{\delta})/\lambda} \quad (8)$$

otherwise.

Finally, leveraging [16], [36]–[38], the bistatic RCS of a forward reflecting element is modeled as

$$\bar{\zeta}(\varphi_{\text{in}}, \varphi_{\text{out}}) = \underbrace{\bar{A}[\cos(\varphi_{\text{in}}^{\text{az}})\cos(\varphi_{\text{in}}^{\text{el}})]^q}_{\bar{\zeta}_a(\varphi_{\text{in}})} \times \underbrace{(4\pi\bar{A}/\lambda^2)[\cos(\varphi_{\text{out}}^{\text{az}})\cos(\varphi_{\text{out}}^{\text{el}})]^q}_{\bar{\zeta}_g(\varphi_{\text{out}})} \quad (9)$$

if $\varphi_{\text{in}}^{\text{az}}, \varphi_{\text{in}}^{\text{el}}, \varphi_{\text{out}}^{\text{az}}, \varphi_{\text{out}}^{\text{el}} \in (-\pi/2, \pi/2)$ and $\bar{\zeta}(\varphi_{\text{in}}, \varphi_{\text{out}}) = 0$ otherwise, with \bar{A} being the area of the element. This is a simple yet realistic model, wherein the RCS is regarded as the

product of an effective receive aperture $\bar{\zeta}_a(\varphi_{\text{in}})$ and a transmit gain $\bar{\zeta}_g(\varphi_{\text{out}})$, with a cosine-shaped scan loss in both azimuth and elevation. In order to conserve the power, the cosine exponent $q \geq 0$ must be such that the integral of $\bar{\zeta}_g(\varphi_{\text{out}})$ over a sphere does not exceed 4π sr. This model treats the RIS as a reciprocal surface, i.e., $\bar{\zeta}(\varphi_{\text{in}}, \varphi_{\text{out}}) = \bar{\zeta}(\varphi_{\text{out}}, \varphi_{\text{in}})$, and, at broadside, the entire reflecting area is equal to the sum of the effective apertures of the building elements, so that the overall RIS behaves as a flat plate of area $\bar{N}_s\bar{A}$ [32]. The model in (9) is also used for $\check{\zeta}(\varphi_{\text{in}}, \varphi_{\text{out}})$ upon replacing \bar{A} with the area \check{A} of a backward reflecting element.

III. SYSTEM DESIGN

Let $\mathbf{f} \in \mathbb{C}^{\bar{N}_r\bar{N}_r}$ be the unit-norm filter employed by the receiver to focus the radar towards the location under inspection, which is under the designer's control; then, its output is

$$r = \mathbf{f}^H e(\bar{\mathbf{x}}, \check{\mathbf{x}})\alpha + \mathbf{f}^H \mathbf{w} \quad (10)$$

resulting in the following SNR

$$\text{SNR} = |\mathbf{f}^H e(\bar{\mathbf{x}}, \check{\mathbf{x}})|^2 \frac{\sigma_\alpha^2}{\sigma_w^2} \quad (11)$$

where $\sigma_\alpha^2 = \mathbb{E}[|\alpha|^2]$. Also, the GLRT discriminating between the target presence (hypothesis H_1) and absence (hypothesis H_0) is [27]

$$\frac{|r|^2}{\sigma_w^2} \underset{H_0}{\overset{H_1}{\geq}} \eta \quad (12)$$

where $\eta > 0$ is the detection threshold, to be set according to the desired probability of false alarm $P_{\text{fa}} = e^{-\eta}$; assuming that $|\alpha|^2$ is non fluctuating, exponentially distributed, or gamma distributed with variance $\sigma_\alpha^2/2$, the corresponding detection probabilities are [28], [35]

$$P_d = \begin{cases} Q_1(\sqrt{2\text{SNR}}, \sqrt{2\eta}) & \text{(non fluctuating)} \\ e^{-\eta/(1+\text{SNR})} & \text{(exponential)} \\ \left(1 + \frac{\gamma\text{SNR}/2}{(1+\text{SNR}/2)^2}\right) e^{-\eta/(1+\text{SNR}/2)} & \text{(gamma)}. \end{cases} \quad (13)$$

where $Q_1(\cdot, \cdot)$ is the Marcum's Q -function.

The receive filter and the phase shifts of the RIS can be jointly chosen to maximize the SNR at the location under inspection and, as a by product, the detection probability in (13). For any $\bar{\mathbf{x}}$ and $\check{\mathbf{x}}$, the optimal filter is the one matched to the signal to be detected, i.e.,

$$\mathbf{f} = \frac{e(\bar{\mathbf{x}}, \check{\mathbf{x}})}{\|e(\bar{\mathbf{x}}, \check{\mathbf{x}})\|}. \quad (14)$$

Hence, upon plugging (14) into (11), the optimal phase shifts are obtained as the solution to

$$\begin{aligned} \max_{\bar{\mathbf{x}}, \check{\mathbf{x}}} \quad & \|e(\bar{\mathbf{x}}, \check{\mathbf{x}})\|^2 \\ \text{s.t.} \quad & |\bar{x}_n| = 1, \quad n = 1, \dots, \bar{N}_s \\ & |\check{x}_n| = 1, \quad n = 1, \dots, \bar{N}_s \end{aligned} \quad (15)$$

which is independent of the target and noise strength (namely, of σ_α^2 and σ_w^2). Notice that the design in (15) can be regarded as a form of passive beamforming. Indeed, by acting on the

response of the forward and backward reflecting elements, the indirect steering vectors of the radar transmitter and receiver towards the target can be modified to provide an SNR gain, respectively; such gain results from the constructive alignment of the indirect signals reflected by each element of the RIS and of the direct signal during both the illumination and the observation of the target. Since the objective function $\|e(\bar{x}, \bar{x})\|^2 = \|\bar{e}(\bar{x})\|^2 \|\bar{e}(\bar{x})\|^2$ and the constraint set in (15) are separable with respect to the variables \bar{x} and \bar{x} , the forward and backward phase shifts can be optimized independently; specifically, the problems to be solved are

$$\max_{\bar{x}} \|\bar{e}(\bar{x})\|^2, \quad \text{s.t. } |\bar{x}_n| = 1, \quad n = 1, \dots, \bar{N}_s \quad (16)$$

when the forward RIS is present, and

$$\max_{\bar{x}} \|\bar{e}(\bar{x})\|^2, \quad \text{s.t. } |\bar{x}_n| = 1, \quad n = 1, \dots, \bar{N}_s \quad (17)$$

when the backward RIS is present.

A. Optimization of the phase shifts of the RIS

We discuss here the solution to (16), while similar arguments can be used to tackle (17). Let $\bar{\mathbf{y}} = \bar{\mathbf{v}}_r \bar{\gamma}_r$ and $\bar{\mathbf{Q}} = \bar{\mathbf{G}} \text{diag}(\bar{\mathbf{v}}_s) \bar{\gamma}_s$, which are computed based only on the knowledge of the system geometry (i.e., the position of the radar transmit elements and the forward-reflecting elements, which are available), the location to be inspected (which is decided by the radar engineer), the radar-RIS channel (which can be estimated in advance), and the far-field path-loss model (which can be obtained from experimental data and/or theoretical models). Problem (16) is now rewritten as

$$\max_{\bar{x}} \|\bar{\mathbf{y}} + \bar{\mathbf{Q}}\bar{x}\|^2, \quad \text{s.t. } |\bar{x}_n| = 1, \quad n = 1, \dots, \bar{N}_s. \quad (18)$$

When $\text{rank}(\bar{\mathbf{Q}}) = 1$, which occurs if the radar transmitter and the forward RIS are in each other's far-field (more on this in Sec. III-B) or $\bar{N}_r = 1$ or $\bar{N}_s = 1$, then the solution to (18) is derived in closed form. Indeed, upon factorizing $\bar{\mathbf{Q}}$ as $\bar{\mathbf{a}}\bar{\mathbf{b}}^T$, with $\bar{\mathbf{a}} \in \mathbb{C}^{\bar{N}_r}$ and $\bar{\mathbf{b}} \in \mathbb{C}^{\bar{N}_s}$, we have that

$$\begin{aligned} \|\bar{\mathbf{y}} + \bar{\mathbf{a}}\bar{\mathbf{b}}^T\bar{x}\|^2 &= \|\bar{\mathbf{y}}\|^2 + \|\bar{\mathbf{a}}\|^2 \left| \sum_{n=1}^{\bar{N}_s} \bar{b}_n \bar{x}_n \right|^2 \\ &\quad + 2\Re \left\{ \bar{\mathbf{y}}^H \bar{\mathbf{a}} \sum_{n=1}^{\bar{N}_s} \bar{b}_n \bar{x}_n \right\} \\ &\leq \|\bar{\mathbf{y}}\|^2 + \|\bar{\mathbf{a}}\|^2 \left(\sum_{n=1}^{\bar{N}_s} |\bar{b}_n| \right)^2 + 2|\bar{\mathbf{y}}^H \bar{\mathbf{a}}| \sum_{n=1}^{\bar{N}_s} |\bar{b}_n| \end{aligned} \quad (19)$$

where the last upper bound is achieved when

$$\angle \bar{x}_n = -\angle \bar{b}_n - \angle(\bar{\mathbf{y}}^H \bar{\mathbf{a}}), \quad n = 1, \dots, \bar{N}_s. \quad (20)$$

When $\text{rank}(\bar{\mathbf{Q}}) > 1$, upon introducing the following positive semi-definite matrix⁷

$$\bar{\mathbf{B}} = \begin{pmatrix} \bar{\mathbf{Q}}^H \bar{\mathbf{Q}} & \bar{\mathbf{Q}}^H \bar{\mathbf{y}} \\ \bar{\mathbf{y}}^H \bar{\mathbf{Q}} & \|\bar{\mathbf{y}}\|^2 \end{pmatrix} \in \mathbb{C}^{(\bar{N}_s+1) \times (\bar{N}_s+1)} \quad (21)$$

⁷The positive-semidefiniteness is verified by exploiting the Schur complement for block matrices.

Algorithm 1 Alternate maximization for Problem (23)

- 1: Choose $\epsilon > 0$, $K_{\max} > 0$, and $\bar{\mathbf{z}} \in \mathbb{C}^{\bar{N}_s+1}$: $|\bar{z}_n| = 1$, $\forall n$
 - 2: $k = 0$ and $\bar{f}_0 = \bar{\mathbf{z}}^H \bar{\mathbf{B}} \bar{\mathbf{z}}$
 - 3: **repeat**
 - 4: **for** $n = 1, \dots, \bar{N}_s + 1$ **do**
 - 5: $\bar{z}_n = \begin{cases} e^{i\angle(\sum_{j \neq n} \bar{B}_{nj} \bar{z}_j)}, & \text{if } \sum_{j \neq n} \bar{B}_{nj} \bar{z}_j \neq 0 \\ 1, & \text{otherwise} \end{cases}$
 - 6: **end for**
 - 7: $k = k + 1$
 - 8: $\bar{f}_k = \bar{\mathbf{z}}^H \bar{\mathbf{B}} \bar{\mathbf{z}}$
 - 9: **until** $\bar{f}_k - \bar{f}_{k-1} < \epsilon \bar{f}_k$ or $k = K_{\max}$
-

Problem (18) is recast as

$$\begin{aligned} \max_{\bar{x}, \phi} \quad & (e^{-i\phi} \bar{\mathbf{x}}^H \quad e^{-i\phi}) \bar{\mathbf{B}} (e^{i\phi} \bar{\mathbf{x}}^T \quad e^{i\phi})^T \\ \text{s.t.} \quad & |\bar{x}_n| = 1, \quad n = 1, \dots, \bar{N}_s \end{aligned} \quad (22)$$

which in turn is equivalent to

$$\max_{\bar{z}} \bar{\mathbf{z}}^H \bar{\mathbf{B}} \bar{\mathbf{z}}, \quad \text{s.t. } |\bar{z}_n| = 1, \quad n = 1, \dots, \bar{N}_s + 1. \quad (23)$$

If $\bar{\mathbf{z}}^*$ solves (23), the solution to (18) can be recovered as $\angle \bar{x}_n = \angle \bar{z}_n^* - \angle \bar{z}_{\bar{N}_s+1}^*$, $n = 1, \dots, \bar{N}_s$. Problem (23) is a complex quadratic program, that is strongly NP-hard in general [39], [40]. A sub-optimal solution can be obtained via an alternate maximization, as reported in Algorithm 1 [41]. In this case, one entry of $\bar{\mathbf{z}}$ at a time is iteratively optimized; since $|\bar{z}_n| = 1$ for any n , the objective function of (23) can be written as $2\Re\{\bar{z}_n^* \sum_{j \neq n} \bar{B}_{nj} \bar{z}_j\} + \bar{B}_{nn} + \sum_{k \neq n} \sum_{j \neq n} \bar{z}_k^* \bar{B}_{kj} \bar{z}_j$, and the constrained maximization over \bar{z}_n gives

$$\bar{z}_n = e^{i\angle(\sum_{j \neq n} \bar{B}_{nj} \bar{z}_j)} \quad (24)$$

if $\sum_{j \neq n} \bar{B}_{nj} \bar{z}_j \neq 0$, and any unit modulus complex number, otherwise. Since the objective function is bounded above and monotonically increased at each iteration, convergence is ensured. The complexity per iteration is $\mathcal{O}(\bar{N}_s^2)$, with an initial cost of $\mathcal{O}(\bar{N}_s^3)$ to form the matrix $\bar{\mathbf{B}}$ in (21).

Alternatively (see, e.g., [39], [40], [42]–[44]), Problem (23) can be reformulated as

$$\begin{aligned} \max_{\bar{\mathbf{Z}}, \bar{\mathbf{z}}} \quad & \text{Tr}(\bar{\mathbf{B}} \bar{\mathbf{Z}}) \\ \text{s.t.} \quad & \bar{Z}_{nn} = 1, \quad n = 1, \dots, \bar{N}_s + 1 \\ & \bar{\mathbf{Z}} \succeq 0, \quad \bar{\mathbf{Z}} = \bar{\mathbf{z}} \bar{\mathbf{z}}^H \end{aligned} \quad (25)$$

that admits the following (convex) relaxation

$$\begin{aligned} \max_{\bar{\mathbf{Z}}} \quad & \text{Tr}(\bar{\mathbf{B}} \bar{\mathbf{Z}}) \\ \text{s.t.} \quad & \bar{Z}_{nn} = 1, \quad n = 1, \dots, \bar{N}_s + 1, \quad \bar{\mathbf{Z}} \succeq 0 \end{aligned} \quad (26)$$

which can be solved by standard techniques, such as interior point methods, first-order methods on the associated dual problem, block coordinate ascent, etc. Let $\bar{\mathbf{Z}}^*$ be the solution to (26); as shown in [39], [41], [43], a sub-optimum solution $\bar{\mathbf{z}}$ to (23) can be obtained by generating a sample vector from a complex zero-mean circularly symmetric Gaussian distribution with covariance matrix $\bar{\mathbf{Z}}^*$ and by normalizing its entries to have a unit modulus. This randomized algorithm satisfies a

noticeable property: indeed, letting \bar{f}^* be the optimal value of the objective function in (23), we have [39], [40]

$$\text{Tr}(\bar{\mathbf{B}}\bar{\mathbf{Z}}^*) \geq \bar{f}^* \geq \text{E}[\bar{s}^H \bar{\mathbf{B}} \bar{s}] \geq \frac{\pi}{4} \text{Tr}(\bar{\mathbf{B}}\bar{\mathbf{Z}}^*) \quad (27)$$

which shows that this is a randomized $\frac{\pi}{4}$ -approximation algorithm.⁸ Clearly, multiple (independent) feasible points \bar{s} can be computed, and the one providing the largest objective function in (23) can be chosen: in this case, the $\frac{\pi}{4}$ approximation ratio will not only hold in mean but also with a probability that goes to 1 exponentially fast with the number of samples. The complexity of this approach depends on the technique used to solve Problem (26): e.g., $\mathcal{O}(\bar{N}_s^3)$ per iteration for interior point methods and for the block coordinate ascent algorithm, or $\mathcal{O}(\bar{N}_s^2 \ln \bar{N}_s)$ per iteration for the sub-gradient algorithm on the associated dual problem [41]. Additionally, there is a cost of $\mathcal{O}(\bar{N}_s^3)$ for the evaluation of the square root matrix of $\bar{\mathbf{Z}}^*$ needed in the randomization step.

B. Far-field deployment of the RISs

We study here in more detail the case where the radar transmitter and the forward RIS are in each other's far-field and the radar receiver and the backward RIS are in each other's far-field. In this situation, a plane wave approximation in the aforementioned radar-RIS hops can be made and, hence, the matrices in (7) and (8) simplify to $\bar{\mathbf{G}} = \bar{\mathbf{g}}_r \bar{\mathbf{g}}_s^T$ and $\check{\mathbf{G}} = \check{\mathbf{g}}_r \check{\mathbf{g}}_s^T$, respectively, where $\bar{\mathbf{g}}_r$ is the steering vector of the radar transmitter towards the forward RIS, $\check{\mathbf{g}}_r$ is the steering vector of the radar receiver towards the backward RIS, $\bar{\mathbf{g}}_s$ is the steering vector of the forward RIS towards the radar transmitter, and $\check{\mathbf{g}}_s$ is the steering vector of the backward RIS towards the radar receiver: all these steering vectors are tied to the geometry of the corresponding array and have unit modulus entries. Since the matrix

$$\bar{\mathbf{Q}} = \underbrace{\bar{\mathbf{g}}_r}_{\bar{\mathbf{a}}} \underbrace{\bar{\mathbf{g}}_s^T \text{diag}(\bar{\mathbf{v}}_s) \bar{\gamma}_s}_{\bar{\mathbf{b}}^T} \quad (28)$$

has rank one, upon exploiting (19) and (20), we have that

$$\max_{\bar{\mathbf{x}}} \|\bar{\mathbf{e}}(\bar{\mathbf{x}})\|^2 = \bar{N}_r |\bar{\gamma}_r|^2 + \bar{N}_r \bar{N}_s^2 |\bar{\gamma}_s|^2 + 2\bar{N}_s |\bar{\gamma}_r^* \bar{\gamma}_s| |\bar{\mathbf{v}}_r^H \bar{\mathbf{g}}_r| \quad (29)$$

that is achieved when

$$\bar{\varphi}_n = -\angle(\bar{g}_{s,n} \bar{v}_{s,n} \bar{\gamma}_s) - \angle(\bar{\gamma}_r^* \bar{\mathbf{v}}_r^H \bar{\mathbf{g}}_r), \quad n = 1, \dots, \bar{N}_s. \quad (30)$$

Similarly, we have that

$$\max_{\check{\mathbf{x}}} \|\check{\mathbf{e}}(\check{\mathbf{x}})\|^2 = \check{N}_r |\check{\gamma}_r|^2 + \check{N}_r \check{N}_s^2 |\check{\gamma}_s|^2 + 2\check{N}_s |\check{\gamma}_r^* \check{\gamma}_s| |\check{\mathbf{v}}_r^H \check{\mathbf{g}}_r| \quad (31)$$

that is achieved when

$$\check{\varphi}_n = -\angle(\check{g}_{s,n} \check{v}_{s,n} \check{\gamma}_s) - \angle(\check{\gamma}_r^* \check{\mathbf{v}}_r^H \check{\mathbf{g}}_r), \quad n = 1, \dots, \check{N}_s. \quad (32)$$

⁸A (randomized) α -approximation algorithm is an algorithm that runs in polynomial time and produces a solution whose (expected) value is at least a fraction α of the optimum value [45].

To get some insights into the achievable performance, we now evaluate the optimal SNR under a LOS radar configuration (i.e., $\bar{\gamma}_r \check{\gamma}_r \neq 0$); from (5), (11), (29), and (31), we obtain

$$\begin{aligned} \text{SNR} &= \underbrace{\frac{\bar{N}_r \check{N}_r |\bar{\gamma}_r \check{\gamma}_r|^2 \sigma_\alpha^2}{\sigma_w^2}}_{\text{SNR}_o} \\ &\times \underbrace{\left(1 + \bar{N}_s^2 \frac{|\bar{\gamma}_s|^2}{|\bar{\gamma}_r|^2} + 2\bar{N}_s \frac{|\bar{\gamma}_s|}{|\bar{\gamma}_r|} \frac{|\bar{\mathbf{v}}_r^H \bar{\mathbf{g}}_r|}{\bar{N}_r} \right)}_{\bar{\Gamma}} \\ &\times \underbrace{\left(1 + \check{N}_s^2 \frac{|\check{\gamma}_s|^2}{|\check{\gamma}_r|^2} + 2\check{N}_s \frac{|\check{\gamma}_s|}{|\check{\gamma}_r|} \frac{|\check{\mathbf{v}}_r^H \check{\mathbf{g}}_r|}{\check{N}_r} \right)}_{\check{\Gamma}} \end{aligned} \quad (33)$$

where SNR_o is the SNR when the radar operates alone, while $\bar{\Gamma} > 1$ and $\check{\Gamma} > 1$ are the gain granted by the RIS-aided illumination and observation, respectively. Under the model in (6), we have

$$\begin{aligned} \bar{\Gamma} &\approx 1 + \frac{\bar{\mathcal{G}}(\bar{\rho}) \bar{L}_r \bar{N}_s^2 \bar{\zeta}(\bar{\omega}, \bar{\theta}_s)}{\bar{\mathcal{G}}(\bar{\theta}_r) \bar{L}_s} \frac{1}{4\pi \bar{\delta}^2} \\ &+ 2 \left(\frac{\bar{\mathcal{G}}(\bar{\rho}) \bar{L}_r \bar{N}_s^2 \bar{\zeta}(\bar{\omega}, \bar{\theta}_s)}{\bar{\mathcal{G}}(\bar{\theta}_r) \bar{L}_s} \frac{1}{4\pi \bar{\delta}^2} \right)^{1/2} \frac{|\bar{\mathbf{v}}_r^H \bar{\mathbf{g}}_r|}{\bar{N}_r} \end{aligned} \quad (34a)$$

$$\begin{aligned} \check{\Gamma} &\approx 1 + \frac{\check{\mathcal{G}}(\check{\rho}) \check{L}_r \check{N}_s^2 \check{\zeta}(\check{\theta}_s, \check{\omega})}{\check{\mathcal{G}}(\check{\theta}_r) \check{L}_s} \frac{1}{4\pi \check{\delta}^2} \\ &+ 2 \left(\frac{\check{\mathcal{G}}(\check{\rho}) \check{L}_r \check{N}_s^2 \check{\zeta}(\check{\theta}_s, \check{\omega})}{\check{\mathcal{G}}(\check{\theta}_r) \check{L}_s} \frac{1}{4\pi \check{\delta}^2} \right)^{1/2} \frac{|\check{\mathbf{v}}_r^H \check{\mathbf{g}}_r|}{\check{N}_r} \end{aligned} \quad (34b)$$

where the above approximations follow from the fact that $\bar{d}_r \approx \bar{d}_s$ and $\check{d}_r \approx \check{d}_s$, respectively. Observe now that, we must necessarily have $\bar{\delta} \lambda > 2\bar{D}_s^2$ and $\check{\delta} \lambda > 2\check{D}_s^2$ in order to ensure far-field operation [30]; consequently, assuming that square RISs are employed, so that $\bar{N}_s \bar{A} = \bar{D}_s^2$ and $\check{N}_s \check{A} = \check{D}_s^2$, under the model in (9) we have

$$\frac{\bar{N}_s^2 \bar{\zeta}(\bar{\omega}, \bar{\theta}_s)}{4\pi \bar{\delta}^2} \leq \left(\frac{\bar{N}_s \bar{A}}{\bar{\delta} \lambda} \right)^2 \leq \frac{1}{4} \quad (35a)$$

$$\frac{\check{N}_s^2 \check{\zeta}(\check{\theta}_s, \check{\omega})}{4\pi \check{\delta}^2} \leq \left(\frac{\check{N}_s \check{A}}{\check{\delta} \lambda} \right)^2 \leq \frac{1}{4}. \quad (35b)$$

From (34) and (35) we conclude that, when $\bar{\gamma}_r \check{\gamma}_r \neq 0$, the additional paths enabled by a far-field RIS deployment only provide a marginal SNR gain: the reason is that the reflecting area offered by the RIS cannot be sufficiently large to compensate for the signal attenuation experienced in the radar-RIS hop. As also confirmed by the analysis in Sec. IV, the forward (backward) RIS should better be placed in the near-field of the radar transmit (receive) array, as close as possible, to significantly improve the system performance. Similar conclusions have been reached in communication-oriented applications, when the effects of the double-fading attenuation and of the bistatic RCS of the reflecting elements are accounted for in the RIS-aided link [8], [38].

We hasten to underline that, when the RIS is in the far-field of both the signal source and the destination, many existing

works have bypassed the fact that the indirect link can be much weaker than the direct one by assuming that the latter is obstructed; indeed, such a far-field deployment may remain a competitive option if the indirect link allows to reach a user that would otherwise remain disconnected (in communication applications) or a spot that would otherwise remain blind (in radar applications), in spite of the double-fading attenuation.

C. Mono-static radar with a bi-directional RIS

We study here in more detail a monostatic radar wherein the same RIS helps both the transmitter and the receiver: in this case, we have $\bar{N}_s = \bar{N}_s = N_s$, $(\bar{d}_s, \bar{\theta}_s) = (\bar{d}_s, \bar{\theta}_s)$, $\bar{v}_s = \bar{v}_s$, $\bar{\gamma}_s \bar{\gamma}_s \neq 0$, and $\bar{\zeta}(\cdot, \cdot) = \bar{\zeta}(\cdot, \cdot)$. The disjoint design discussed in Section III-A can directly be employed if the phase shift introduced by each reflecting element can be reprogrammed in between the arrival of the forward (from the radar transmitter) and of the backward (from the target) incident wave. To simplify the hardware, we also discuss next the relevant case where the additional constraint $\bar{x} = \bar{x} = x$ is enforced to (15); accordingly, the design of the phase shifts is recast as

$$\max_{\mathbf{x}} \|e(\mathbf{x}, \mathbf{x})\|^2, \quad \text{s.t. } |x_n| = 1, \quad n = 1, \dots, N_s \quad (36)$$

Notice that forcing $\bar{x} = \bar{x}$ is optimal if $\bar{e}(\cdot) = \bar{e}(\cdot)$: this occurs when the RIS is reciprocal *and* the radar employs the same reciprocal array for both transmission and reception; instead, it is inevitably sub-optimal if the system presents an asymmetry between the transmit and the receive side. In this latter case, we compute a sub-optimal solution to (36) by iteratively optimizing one phase shift at a time. To proceed, the objective function is expanded as

$$\begin{aligned} \|e(\varphi, \varphi)\|^2 &= \|\bar{\mathbf{t}}_n + \bar{\mathbf{q}}_n x_n\|^2 \|\bar{\mathbf{t}}_n + \bar{\mathbf{q}}_n x_n\|^2 \\ &= (\|\bar{\mathbf{t}}_n\|^2 + \|\bar{\mathbf{q}}_n\|^2) (\|\bar{\mathbf{t}}_n\|^2 + \|\bar{\mathbf{q}}_n\|^2) \\ &\quad + 2(\|\bar{\mathbf{t}}_n\|^2 + \|\bar{\mathbf{q}}_n\|^2) \Re \{ \bar{\mathbf{t}}_n^H \bar{\mathbf{q}}_n x_n \} \\ &\quad + 2(\|\bar{\mathbf{t}}_n\|^2 + \|\bar{\mathbf{q}}_n\|^2) \Re \{ \bar{\mathbf{t}}_n^H \bar{\mathbf{q}}_n x_n \} \\ &\quad + 4\Re \{ \bar{\mathbf{t}}_n^H \bar{\mathbf{q}}_n \bar{\mathbf{t}}_n^H \bar{\mathbf{q}}_n x_n^2 \} \end{aligned} \quad (37)$$

where $\bar{\mathbf{q}}_n$ is the n -th column of the matrix $\bar{\mathbf{G}} \text{diag}(\bar{v}_s) \bar{\gamma}_s$, and $\bar{\mathbf{t}}_n = \bar{\gamma}_r \bar{v}_r + \sum_{j=1, j \neq n}^{N_s} \bar{\mathbf{q}}_j x_j$ at the transmit side, and $\bar{\mathbf{q}}_n$ is the n -th column of the matrix $\bar{\mathbf{G}} \text{diag}(\bar{v}_s) \bar{\gamma}_s$ and $\bar{\mathbf{t}}_n = \bar{\gamma}_r \bar{v}_r + \sum_{j=1, j \neq n}^{N_s} \bar{\mathbf{q}}_j x_j$ at the receive side. Neglecting the irrelevant terms in (37), the problem to be solved becomes

$$\max_{\varphi_n} \Re \{ A_n e^{i\varphi_n} + B_n e^{i2\varphi_n} \} \quad (38)$$

where $x_n = e^{i\varphi_n}$, $A_n = 2(\|\bar{\mathbf{t}}_n\|^2 + \|\bar{\mathbf{q}}_n\|^2) \bar{\mathbf{t}}_n^H \bar{\mathbf{q}}_n + 2(\|\bar{\mathbf{t}}_n\|^2 + \|\bar{\mathbf{q}}_n\|^2) \bar{\mathbf{t}}_n^H \bar{\mathbf{q}}_n$ and $B_n = 4\bar{\mathbf{t}}_n^H \bar{\mathbf{q}}_n \bar{\mathbf{t}}_n^H \bar{\mathbf{q}}_n$. The overall procedure is summarized in Algorithm 2: since the value of the objective function is bounded above and monotonically increased at each iteration, convergence is ensured. Finally, notice that the solution to (38) can be found among the zeros of the derivative of the objective function, i.e., $|A_n| \sin(\varphi_n + \angle A_n) + 2|B_n| \sin(2\varphi_n + \angle B_n)$, which can be obtained numerically.

Algorithm 2 Alternate maximization for Problem (36)

- 1: Choose $\epsilon > 0$, $K_{\max} > 0$, and $\mathbf{x} \in \mathbb{C}^{N_s}$: $|x_n| = 1, \forall n$
 - 2: $k = 0$ and $f_0 = 0$
 - 3: **repeat**
 - 4: **for** $n = 1, \dots, N_s$ **do**
 - 5: $\angle x_n = \arg \max_{\varphi} \Re \{ A_n e^{i\varphi} + B_n e^{i2\varphi} \}$
 - 6: **end for**
 - 7: $k = k + 1$
 - 8: $f_k = \|e(\mathbf{x}, \mathbf{x})\|^2$
 - 9: **until** $f_k - f_{k-1} < \epsilon f_k$ or $k = K_{\max}$
-

D. More insights on the radar and RIS interplay

An MIMO radar emitting orthogonal waveforms simultaneously illuminates a large angular sector, whose width is tied to the beampattern of the transmit antennas; when operating alone, this radar can be focused on a desired point in the illuminated region by only relying on receive signal processing, and multiple points can be simultaneously inspected by changing the range gate and the receive filter.

An RIS-aided MIMO radar benefits from additional degrees of freedom, namely, the choice of the phase shifts of the reflecting elements and a modified field of view. Since an RIS must be programmed before the transmission of the radar waveforms, the system engineer must decide in advance how it should operate. The design proposed in (15) chooses the phase shifts of both the forward and the backward RIS in order to enhance the SNR at only one desired location. For example, the location of interest can be the one where an alert was previously found (if the radar is operating in an alert/confirm mode [46]) or the one where a previously-detected target is expected to be found (if the radar is operating in a tracking mode) or a spot not accessible by the radar when operating alone [25]. Even if the RISs are optimized to look at only one location, the radar can still simultaneously inspect other spots.

Needless to say, different design criteria could be also considered to operate the RIS-aided MIMO radar. For example, the forward and backward RISs could be steered towards multiple, possibly different locations, which may be of interest in the presence of multiple targets.

IV. PERFORMANCE ANALYSIS

We present here some examples to assess the performance achievable by an RIS-aided MIMO radar. The analysis is carried out under the model in Sec. II-D, with $\bar{L}_r = \bar{L}_s = \bar{L}_r = \bar{L}_s$ in (6). The RIS design is undertaken by resorting to Algorithms 1 and 2, which are implemented with $K_{\max} = 200$, $\epsilon = 10^{-5}$, and 100 random initialization points.⁹

A. System geometry

We consider the geometry in Fig. 2, which features a bistatic radar operating at 3 GHz, aided by a forward and/or backward RIS.¹⁰ The radar transmitter and receiver employ a linear array

⁹In the following examples, the alternate maximization and the semi-definite relaxation with randomization discussed in Section III-A have provided similar values of the objective function in Problem (23).

¹⁰The S-band (2÷4 GHz) is used for example by airport surveillance radars, weather radars, and surface ship radars, which can cover up to 100 km.

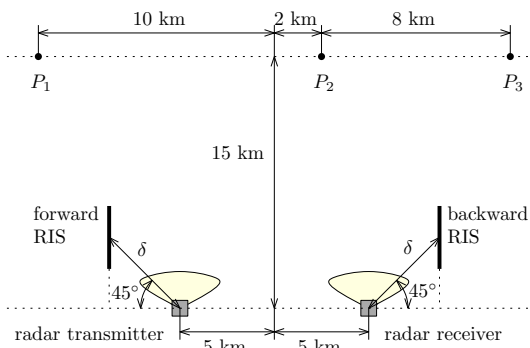


Figure 2. Considered system geometry. The radar transmitter and receiver and the forward and backward RISs are equipped with planar arrays; their local x and y axes lay on the same plane, which also contains the array centers and the prospective target. The target is either fixed at P_2 or moved along the line segment connecting P_1 to P_3 (from left to right).

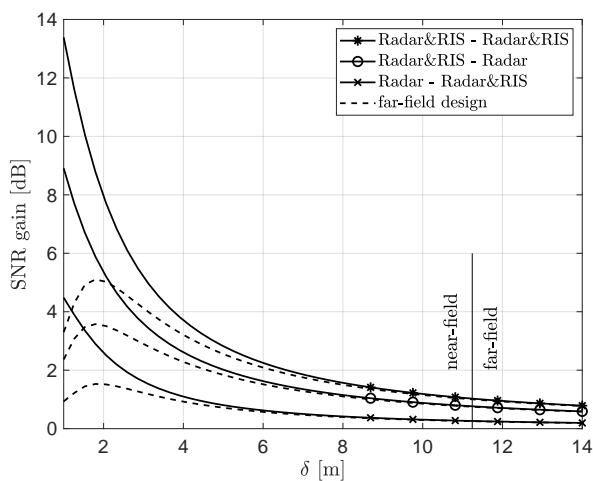


Figure 3. SNR gain (as compared to case where the radar operates alone) obtained by using a forward and/or a backward RIS versus δ , when $N_s = 225$. The system geometry in Fig. 2 is considered with the target located at P_2 .

with a $\lambda/2$ element spacing along the local y -axis, $\bar{N}_r = 3$, and (unless otherwise stated) $\bar{N}_r = 8$; each array element has a rectangular shape of size $\lambda/2$ and λ along the local y and z axes, respectively, and a power beampattern with a 3-dB width of 120° in azimuth and of 60° in elevation. The RISs (if present) have a square shape and are composed of $\bar{N}_s = \bar{N}_s = N_s$ adjacent square elements with an area $\bar{A} = \bar{A} = \lambda^2/4$ and a cosine exponent $q = 1$ in (9); this may for example correspond to a reflectarray-based RIS implementation [2]. The reference element of each array is at the center of the array, with $\bar{\delta} = \bar{\delta} = \delta$, while the target has an effective size of $\bar{D}_t = \bar{D}_t = 10\lambda$. Unless otherwise stated, we report next the performance when the target is at P_2 and the RISs are designed to maximize the SNR at this same location.

B. Impact of the radar-RIS distance

We first study the system behavior when δ is varied and $N_s = 225$. Fig. 3 reports the SNR gain obtained by using a forward and a backward RIS, a forward RIS only, and a backward RIS only, as compared to the case where the radar operates alone (i.e., only the “Radar→Target→Radar”

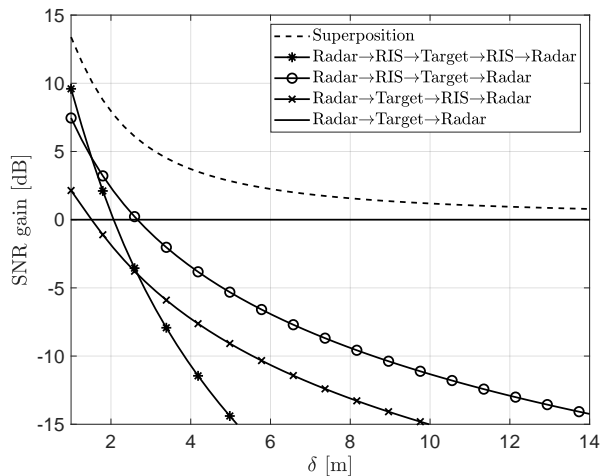


Figure 4. SNR gain (as compared to case where the radar operates alone) of the four echoes in (5) and of their superposition versus δ , when both RIS are employed (“Radar&RIS - Radar&RIS” case) and $N_s = 225$. The system geometry in Fig. 2 is considered with the target located at P_2 .

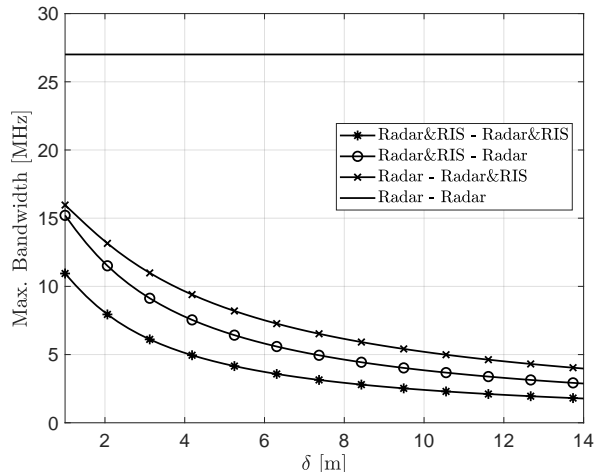


Figure 5. Maximum bandwidth ensuring that the delays of all target echoes reaching the receiver are not resolvable versus δ . The system geometry in Fig. 2 is considered with the target located at P_2 .

echo is present): the configurations considered here correspond to the “Radar&RIS - Radar&RIS”, “Radar&RIS - Radar”, and “Radar - Radar&RIS” cases¹¹ reported in Table I. For comparison, we include the performance obtained with the far-field design in (30) and (32). It is seen that a larger SNR gain is obtained when the radar and RIS get closer, and, in this regime, the far-field design turns out to be detrimental. The SNR gain becomes instead negligible when the radar and RIS arrays are located in each other’s far-field at both the transmit and the receive side, which approximately occurs when $\delta \geq 11.5$ m in this example (as indicated by the vertical dotted line). Simultaneously using a forward and a backward RIS almost doubles the gain as compared to using a single reflecting array. If only a single RIS has to be employed (e.g.,

¹¹The label “Radar - Radar&RIS” indicates that the target is illuminated by the radar and observed by both the radar and the RIS; the meaning of “Radar&RIS - Radar&RIS” and “Radar&RIS - Radar” is similarly understood.

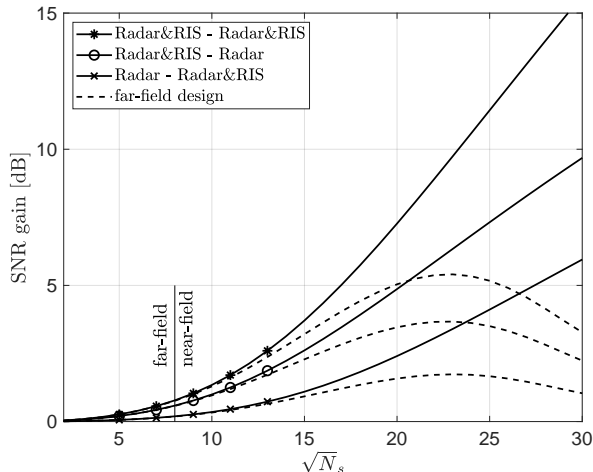


Figure 6. SNR gain (as compared to case where the radar operates alone) obtained by using a forward and/or a backward RIS versus $\sqrt{N_s}$, when $\delta = 4$ m. The system geometry in Fig. 2 is considered with the target located at P_2 .

due to cost constraints), then, for the considered scenario, it should be that at the transmit side: this is a consequence of the fact that the reflecting elements of the forward RIS offer a larger bistatic RCS towards P_2 than those of the forward counterpart. To get further insights, in Fig. 4 we consider the case where both RISs are simultaneously employed and report the SNR gain of the four echoes in (5) and of their superposition. The “Radar→RIS→Target→Radar” echo is stronger than “Radar→Target→RIS→Radar” echo, in keeping with the fact that the elements of the forward RIS offer a larger bistatic RCS towards P_2 ; also, the “Radar→RIS→Target→RIS→Radar” echo is dominant when the distance between the radar and RIS arrays is very small, but it more rapidly fades out when δ is increased due to the more severe path-loss. Finally, Fig. 5 reports the maximum bandwidth compatible with the required narrow-band assumption; this value have been computed as $0.1/(\tau_{\max} - \tau_{\min})$, where τ_{\max} and τ_{\min} are the maximum and the minimum propagation delays from the transmit to the receive elements. Not surprisingly, the maximum bandwidth decreases as δ and/or the number of hops are increased.

C. Impact of the RIS size

Next, we study the system behavior when the number of reflecting elements along each dimension, i.e., $\sqrt{N_s}$, is varied. Fig. 6 reports the SNR gain granted by the use of a forward and/or a backward RIS, as compared to the case where the radar operates alone; the gain increases as the reflecting surfaces get larger; however, it is important to notice that, as long as $\sqrt{N_s} < 8$, the radar and RIS arrays remain in each other’s far-field (as indicated by the vertical dotted line) and only marginal gains are obtained; when instead $\sqrt{N_s}$ gets larger, the advantage of using one or two RISs becomes evident. To further investigate this phenomenon, in Fig. 7 we consider the case where both RISs are simultaneously employed and report the SNR gain of the four echoes in (5) and of their superposition. It is seen that the indirect echoes

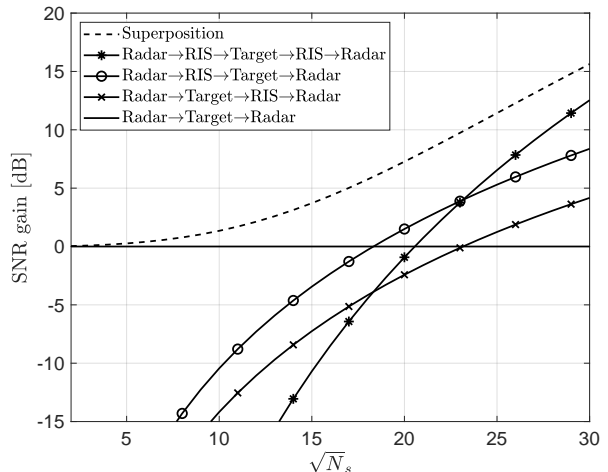


Figure 7. SNR gain (as compared to case where the radar operates alone) of the four echoes in (5) and of their superposition versus $\sqrt{N_s}$, when $\delta = 4$ m and both RIS are employed (“Radar&RIS - Radar&RIS” case). The system geometry in Fig. 2 is considered with the target located at P_2 .

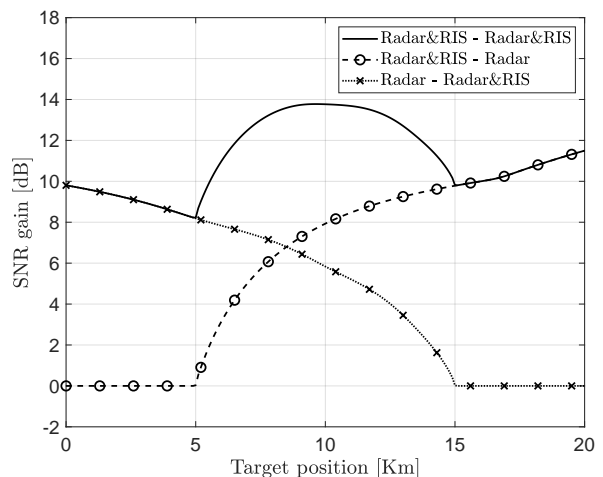


Figure 8. SNR gain (as compared to case where the radar operates alone) obtained by using a forward and/or a backward RIS versus the target position along the line segment going from P_1 ($= 0$ Km) to P_3 ($= 20$ Km), when $N_s = 225$, $\delta = 1$ m, and the system geometry in Fig. 2 is considered.

become progressively stronger as the RIS size is increased and, eventually, dominate over the direct one; hence, upon fixing the distance from the radar, exploiting a reflecting surface becomes competitive only if its size is sufficiently large so as to positively balance the more severe attenuation over this path. In practice, the RIS size is limited by cost and installation constraints; also, it remains understood that complementing an existing radar with a one or more RISs can be attractive only if the cost is inferior to that of upgrading the radar itself with a better performing transceiver.

D. Impact of the target position

We now investigate the system performance as a function of the target position, which is moved along the line segment connecting P_1 to P_3 (from left to right), which has a length of 20 Km, when $N_s = 225$ and $\delta = 1$ m. At first, we

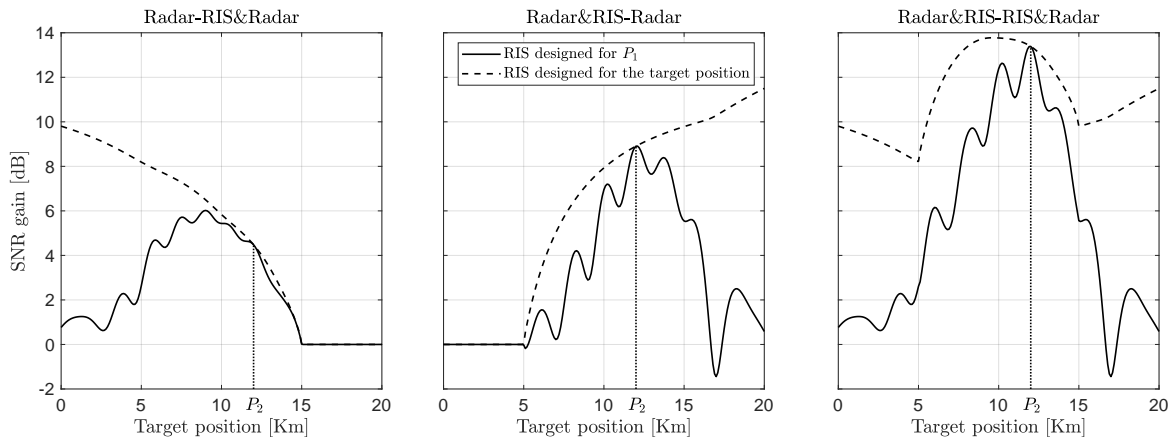


Figure 9. SNR gain (as compared to case where the radar operates alone) when using a forward RIS (left) or a backward RIS (center) or both RIS (right) versus the target position along the line segment going from P_1 ($= 0$ Km) to P_3 ($= 20$ Km), when $N_s = 225$, $\delta = 1$ m, and the system geometry in Fig. 2 is considered. The RISs are designed to maximize the SNR at P_2 ($= 12$ Km) or at the actual target position.

assume that the RISs are designed to maximize the SNR at the actual target location and, in Fig. 8, report the corresponding SNR gain. Notice that the forward RIS cannot illuminate the target in the interval $0 \div 5$ Km; accordingly, the “Radar&RIS–Radar” configuration does not provide any gain here, while the “Radar&RIS–Radar&RIS” and “Radar–Radar&RIS” configurations present the same gain. Similarly, the backward RIS cannot observe the target in the interval $15 \div 20$ Km; accordingly, the “Radar–Radar&RIS” is not effective here, while the “Radar&RIS–Radar&RIS” and “Radar–RIS&Radar” are equivalent. In between, the system can greatly benefit from the simultaneous use of two RISs, in keeping with the results shown in the previous examples. The observed asymmetry in the reported gains, with respect to the middle point of the line segment, is due to the fact that $\tilde{N}_r \neq \hat{N}_r$. Finally, Fig. 9 reports the performance when the RISs are designed to maximize the SNR at P_2 (marked here with a dotted vertical line); for comparison, it also reports the achievable performance when the RISs are designed to maximize the SNR at the actual target location. Even under a mismatched design, a noticeable gain is observed across a large region around P_2 , which progressively reduces by moving away; the observed ripple is due to the fact that the direct and indirect echoes may not always add constructively at locations other than P_2 and, indeed, a small negative gain may even occur occasionally. Overall, the results in Fig. 9 reinforce the intuition that the system engineer can opportunistically activate the available reflecting surfaces to redirect part of the radiated/received power towards/from specific spots to locally boost the detection performance, while the radar transceiver can still keep looking at other regions with acceptable loss, which appears to be a nice feature.

E. Mono-static radar configuration

We assume here that the receive array is co-located with the transmit array and the same RIS is employed for both forward and backward reflection; all other parameters remain defined as in Sec. IV-A. Fig. 10 reports the SNR gain obtained when the forward and backward phase shifts of each reflecting

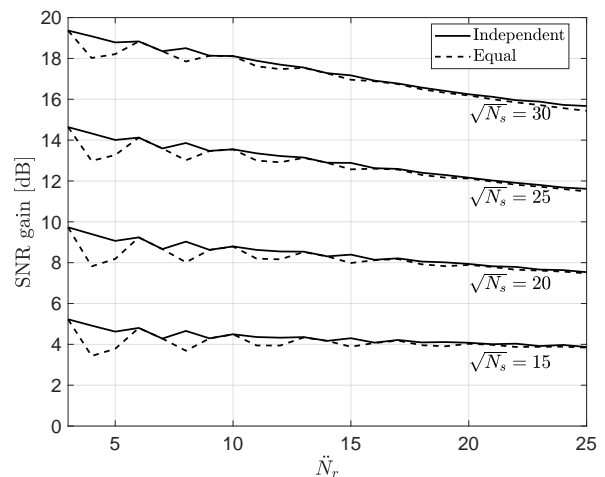


Figure 10. SNR gain (as compared to case where the radar operates alone) versus \tilde{N}_r , when the forward and backward phase shifts are independently optimized or are forced to be equal, $\sqrt{N_s} = 15, 20, 25, 30$ and $\delta = 4$ m. The system geometry in Fig. 2 is modified by moving the receiver to the same location of the transmitter and by using a single bi-directional RIS; the target is located at P_2

element are independently optimized or forced to be equal, as a function of the number of receive elements and for different RIS sizes, when $d = 4$ m. Remarkably, enforcing equal phase values only incurs marginal losses, thus simplifying the required hardware. Also, the obtained SNR gain reduces as \tilde{N}_r is increased; indeed, if the radar is equipped with a better receiver, the reward for using a nearby RIS will be less.

V. CONCLUSIONS

In this work we have started unveiling the benefits of complementing a MIMO radar with RISs placed close to the transmitter/receiver. We have derived a general signal model, which includes monostatic, bistatic, LOS, and NLOS radar configurations and accounts for the presence of up to four paths from the transmitter to the prospective target to the receiver, and have recognized that the reflecting surfaces can

be employed to enhance the achievable detection performance by redirecting/concentrating the radiated power towards/from a specific spot. Our analysis have confirmed a simple intuition: an RIS should be better placed as close as possible to the radar transmitter/receiver in order to limit the additional path loss experienced by an indirect link, with a far-field deployment only providing a marginal advantage when the radar already has a direct view of the target. Also, in a monostatic configuration, the same surface can be used for both forward and backward reflection by simply maintaining the same phase shift, which greatly simplifies its construction and control.

Future works should study the effect of the clutter on the system design and the joint design of the emitted space-time waveforms, the RISs phase shifts, and the receive filter; also, they might consider how to point the RISs towards multiple spots (widely or closely spaced). Moreover, the impact of the mutual coupling among the RIS elements and among the RIS and radar arrays should be investigated; initial efforts in this direction have been done in [47], [48], where a circuit-based end-to-end model is developed for a RIS-aided communication channel; however, the RIS-aided radar channel may be substantially different, as it entails additional hops and passes through a non-cooperative object (namely, the target). Future developments might also investigate applications involving a high-resolution radar where the direct and indirect echoes have resolvable delays or a passive/opportunistic radar exploiting an RIS to redirect the signal emitted by another (possibly non directional) source. A farther research line is studying if and how the estimation of the target parameters and the resolution of closely-spaced objects can improve in the presence of RISs. Finally, the use of active RISs have been recently proposed for future 6G wireless communications [7], [8], and their potential in the context of radar systems remains to be investigated.

REFERENCES

- [1] M. Di Renzo *et al.*, "Smart radio environments empowered by reconfigurable intelligent surfaces: How it works, state of research, and the road ahead," *IEEE Journal on Selected Areas in Communications*, vol. 38, no. 11, pp. 2450–2525, 2020.
- [2] M. A. ElMossallamy *et al.*, "Reconfigurable intelligent surfaces for wireless communications: Principles, challenges, and opportunities," *IEEE Transactions on Cognitive Communications and Networking*, vol. 6, no. 3, pp. 990–1002, Sep. 2020.
- [3] Y. Liu *et al.*, "Reconfigurable intelligent surfaces: Principles and opportunities," *IEEE Communications Surveys & Tutorials*, vol. 2, no. 3, pp. 1546–1577, 2021.
- [4] S. Foo, "Liquid-crystal reconfigurable metasurface reflectors," in *2017 IEEE International Symposium on Antennas and Propagation & USNC/URSI National Radio Science Meeting*, 2017, pp. 2069–2070.
- [5] C. Liaskos, A. Tsioliaridou, A. Pitsillides, S. Ioannidis, and I. Akyildiz, "Using any surface to realize a new paradigm for wireless communications," *Communications of the ACM*, vol. 61, no. 11, pp. 30–33, 2018.
- [6] S. V. Hum and J. Perruisseau-Carrier, "Reconfigurable reflectarrays and array lenses for dynamic antenna beam control: A review," *IEEE Transactions on Antennas and Propagation*, vol. 62, no. 1, pp. 183–198, Jan. 2014.
- [7] R. Long, Y.-C. Liang, Y. Pei, and E. G. Larsson, "Active reconfigurable intelligent surface-aided wireless communications," *IEEE Transactions on Wireless Communications*, vol. 20, no. 8, pp. 4962–4975, Aug. 2021.
- [8] Z. Zhang *et al.*, "Active RIS vs. passive RIS: Which will prevail in 6G?" *arXiv:2103.15154*, 2021. [Online]. Available: <http://arxiv.org/abs/2103.15154>
- [9] M. Di Renzo *et al.*, "Reconfigurable intelligent surfaces vs. relaying: Differences, similarities, and performance comparison," *IEEE Open Journal of the Communications Society*, vol. 1, pp. 798–807, 2020.
- [10] Q. Wu and R. Zhang, "Intelligent reflecting surface enhanced wireless network via joint active and passive beamforming," *IEEE Transactions on Wireless Communications*, vol. 18, no. 11, pp. 5394–5409, Nov. 2019.
- [11] H. Zhang, B. Di, L. Song, and Z. Han, "Reconfigurable intelligent surfaces assisted communications with limited phase shifts: How many phase shifts are enough?" *IEEE Transactions on Vehicular Technology*, vol. 69, no. 4, pp. 4498–4502, Apr. 2020.
- [12] R. Karasik, O. Simeone, M. Di Renzo, and S. Shamai Shitz, "Beyond max-SNR: Joint encoding for reconfigurable intelligent surfaces," in *2020 IEEE International Symposium on Information Theory*, 2020, pp. 2965–2970.
- [13] J. Ye, S. Guo, and M.-S. Alouini, "Joint reflecting and precoding designs for SER minimization in reconfigurable intelligent surfaces assisted MIMO systems," *IEEE Transactions on Wireless Communications*, vol. 19, no. 8, pp. 5561–5574, Aug. 2020.
- [14] J. Mirza and B. Ali, "Channel estimation method and phase shift design for reconfigurable intelligent surface assisted MIMO networks," *IEEE Transactions on Cognitive Communications and Networking*, vol. 7, no. 2, pp. 441–451, Jun. 2021.
- [15] L. Zhao, Z. Wang, and X. Wang, "Wireless power transfer empowered by reconfigurable intelligent surfaces," *IEEE Systems Journal*, 2020.
- [16] V. Jamali, A. M. Tulino, G. Fischer, R. R. Müller, and R. Schober, "Intelligent surface-aided transmitter architectures for millimeter-wave ultra massive MIMO systems," *IEEE Open Journal of the Communications Society*, vol. 2, pp. 144–167, 2021.
- [17] S. Zeng, H. Zhang, B. Di, Z. Han, and L. Song, "Reconfigurable intelligent surface (RIS) assisted wireless coverage extension: RIS orientation and location optimization," *IEEE Communications Letters*, vol. 25, no. 1, pp. 269–273, Jan. 2021.
- [18] H. Wymeersch, J. He, B. Denis, A. Clemente, and M. Juntti, "Radio localization and mapping with reconfigurable intelligent surfaces: Challenges, opportunities, and research directions," *IEEE Vehicular Technology Magazine*, vol. 15, no. 4, pp. 52–61, Oct. 2020.
- [19] A. Elzanaty, A. Guerra, F. Guidi, and M. Alouini, "Reconfigurable intelligent surfaces for localization: Position and orientation error bounds," *IEEE Transactions on Signal Processing*, vol. 69, pp. 5386–5402, 2021.
- [20] A. Fascista, A. Coluccia, H. Wymeersch, and G. Seco-Granados, "RIS-aided joint localization and synchronization with a single-antenna mmwave receiver," in *2021 IEEE International Conference on Acoustics, Speech and Signal Processing*, Jun. 2021, pp. 4455–4459.
- [21] J. He, H. Wymeersch, T. Sanganuak, O. Silven, and M. Juntti, "Adaptive beamforming design for mmwave RIS-aided joint localization and communication," in *2020 IEEE Wireless Communications and Networking Conference Workshops*, Apr. 2020.
- [22] X. Wang, Z. Fei, J. Guo, Z. Zheng, and B. Li, "RIS-assisted spectrum sharing between MIMO radar and MU-MISO communication systems," *IEEE Wireless Communications Letters*, vol. 10, no. 3, pp. 594–598, Mar. 2021.
- [23] X. Wang, Z. Fei, Z. Zheng, and J. Guo, "Joint waveform design and passive beamforming for RIS-assisted dual-functional radar-communication system," *IEEE Transactions on Vehicular Technology*, vol. 70, no. 5, pp. 5131–5136, May 2021.
- [24] S. Buzzi, E. Grossi, M. Lops, and L. Venturino, "Radar target detection aided by reconfigurable intelligent surfaces," *IEEE Signal Processing Letters*, vol. 28, pp. 1315–1319, 2021.
- [25] A. Aubry, A. De Maio, and M. Rosamilia, "Reconfigurable intelligent surfaces for N-LOS radar surveillance," *arXiv:2104.00456*, 2021. [Online]. Available: <http://arxiv.org/abs/2104.00456>
- [26] W. Lu, B. Deng, Q. Fang, X. Wen, and S. Peng, "Intelligent reflecting surface-enhanced target detection in MIMO radar," *IEEE Sensors Letters*, vol. 5, no. 2, pp. 1–4, Feb. 2021.
- [27] S. M. Kay, *Fundamental of Statistical Signal Processing: Detection Theory*. Prentice Hall, 1993, vol. II.
- [28] M. A. Richards, *Fundamentals of radar signal processing*, 2nd ed. New York, NY, USA: McGraw-Hill, 2005.
- [29] E. Grossi, M. Lops, and L. Venturino, "A new look at the radar detection problem," *IEEE Transactions on Signal Processing*, vol. 64, no. 22, pp. 5835–5847, Nov. 2016.
- [30] W. L. Stutzman and G. A. Thiele, *Antenna Theory and Design*, 3rd ed. New York, NY, USA: John Wiley Sons, 1998.
- [31] B. Friedlander, "Localization of signals in the near-field of an antenna array," *IEEE Transactions on Signal Processing*, vol. 67, no. 15, pp. 3885–3893, Aug. 2019.
- [32] C. A. Balanis, *Advanced Engineering Electromagnetics*, 2nd ed. Hoboken, NJ, USA: Wiley, 2012.

- [33] E. Fishler *et al.*, “Spatial diversity in radars – models and detection performance,” *IEEE Transactions on Signal Processing*, vol. 54, no. 3, pp. 823–838, Mar. 2006.
- [34] J. Li and P. Stoica, *MIMO Radar Signal Processing*, 2nd ed. New York, USA: Wiley, 2009.
- [35] C. P. Meyer and H. A. Mayer, *Radar target detection*. New York, NY, USA: Academic Press, 1973.
- [36] S. W. Ellingson, “Path loss in reconfigurable intelligent surface-enabled channels,” *arXiv:1912.06759*, 2019. [Online]. Available: <http://arxiv.org/abs/1912.06759>
- [37] W. Tang *et al.*, “Wireless communications with reconfigurable intelligent surface: Path loss modeling and experimental measurement,” *IEEE Transactions on Wireless Communications*, vol. 20, no. 1, pp. 421–439, Jan. 2021.
- [38] M. Najafi, V. Jamali, R. Schober, and H. V. Poor, “Physics-based modeling and scalable optimization of large intelligent reflecting surfaces,” *IEEE Transactions on Communications*, vol. 69, no. 4, pp. 2673–2691, Apr. 2021.
- [39] S. Zhang and Y. Huang, “Complex quadratic optimization and semidefinite programming,” *SIAM J. Optimization*, vol. 16, no. 3, pp. 871–890, 2006.
- [40] A. M.-C. So, J. Zhang, and Y. Ye, “On approximating complex quadratic optimization problems via semidefinite programming relaxations,” *Math. Program.*, vol. 110, pp. 93–110, 2007.
- [41] I. Waldspurger, A. d’Aspremont, and S. Mallat, “Approximation algorithms for max-3-cut and other problems via complex semidefinite programming,” *Math. Program.*, vol. 149, pp. 47–81, 2015.
- [42] M. X. Goemans and D. P. Williamson, “Improved approximation algorithms for maximum cut and satisfiability problems using semidefinite programming,” *J. ACM*, vol. 42, no. 6, p. 1115–1145, Nov. 1995.
- [43] M. X. Goemans and D. P. Williamson, “Approximation algorithms for max-3-cut and other problems via complex semidefinite programming,” *J. Computer & System Sciences*, vol. 68, no. 2, pp. 442–470, 2004.
- [44] Z.-Q. Luo and T.-H. Chang, “SDP relaxation of homogeneous quadratic optimization: approximation bounds and applications,” in *Convex Optimization in Signal Processing and Communications*, D. P. Palomar and Y. Eldar, Eds. Cambridge, UK: Cambridge University Press, 2010, ch. 4, pp. 533–564.
- [45] D. S. Hochbaum, Ed., *Approximation Algorithms for NP-Hard Problems*. Boston, MA, USA: PWS Publishing Company, 1997.
- [46] E. Grossi, M. Lops, and L. Venturino, “Two-step sequential detection in agile-beam radars: Performance and tradeoffs,” *IEEE Transactions on Aerospace and Electronic Systems*, vol. 53, no. 5, pp. 2199–2213, Oct. 2017.
- [47] G. Gradoni and M. Di Renzo, “End-to-end mutual coupling aware communication model for reconfigurable intelligent surfaces: An electromagnetic-compliant approach based on mutual impedances,” *IEEE Wireless Communications Letters*, vol. 10, no. 5, pp. 938–942, May 2021.
- [48] X. Qian and M. Di Renzo, “Mutual coupling and unit cell aware optimization for reconfigurable intelligent surfaces,” *IEEE Wireless Communications Letters*, vol. 10, no. 6, pp. 1183–1187, Jun. 2021.